

Graphene–Rubber Layered Functional Composites for Seismic Isolation of Structures

Maria Rosaria Marsico,* Julián Mauricio Londoño Monsalve, Dong-Wook Shin, and Monica Felicia Craciun

Herein, novel graphene-reinforced elastomeric isolators (GREI) are proposed. Elastomeric isolators (EIs) are special devices used for seismic isolation of structures. They are made of alternate layers of steel and rubber (steel-reinforced EI [SREI]), and they position between the structure and its foundations to decouple them. The heavy weight and complex manufacturing process of SREI drives costs up, and this restricts their use to strategic buildings such as hospitals and civic centers. In recent years, alternative materials have been proposed to replace the steel sheets of SREI, e.g., glass or carbon fiber-reinforced EIs (FREIs). However, their mechanical behavior requires further investigation before being implemented in existing and new structures safely. As a promising alternative, GREI is proposed here to overcome the heavy weight and long manufacturing process of SREI and the mechanical limitation of FREI to seismic excitations.

materials for EIs which will result in highly efficient, ultralightweight and low-cost devices. Current technologies for base isolation use steel-reinforced EIs (SREIs) to mitigate earthquake-induced vibrations, and to protect structures as well as their contents.^[1,2] SREIs are made of alternate layers of steel and rubber, and are mainly used in strategic and public buildings due to high cost of designing, production, and installation, e.g., San Francisco City Hall, and Government Office of Toshima Ward in Tokyo. With the exception of Japan which has about 4100 base-isolated commercial and institutional buildings, only a few seismic-prone countries are firmly committed to base isolation methodology (e.g., Turkey and China).^[3]

1. Introduction


Elastomeric isolators (EIs) are devices used to isolate structures from seismic or ground-borne excitations in general. They are stiff vertically yet flexible horizontally, and are interposed between the structure and its foundations to decouple them. The concept of interposing those devices is known as base isolation; it is accepted by all major international seismic codes and enables structures to survive potentially devastating seismic events. However, at present, the use of base isolation technology is restricted primarily to strategic buildings such as hospitals and civic centers due to the high costs associated with their manufacturing, shipping, handling, and installation. To extend the use of this technology to residential and commercial buildings, on a global scale, there is an on-going quest for new

The primary weight in a SREI is due to the reinforcing steel shims which are used to provide the rubber–steel composite with high vertical stiffness, and to the end-steel plates at the bottom and top which are used to secure the device to the structure and the foundations. Reducing the weight of EIs would facilitate the manufacturing, shipping, handling, and installation, and would extend the use of this technology to residential and commercial buildings in many parts of the world. Fiber-reinforced EIs (FREIs) are proposed as a less-expensive alternative to SREI, to reduce weight, cost, and manufacturing process time.^[2,4,5] FREIs are made of layers of rubber reinforced with fiber sheets (e.g., glass or carbon fibers) which are lighter than steel shims.

A number of studies have been conducted to investigate the dynamic behavior of FREIs during earthquakes.^[2–4,6–9] Kelly and Takhirov have conducted a theoretical and experimental analysis on FREI and have defined design criteria which were used to manufacture and to test prototypes. To reduce weight further, FREIs can be installed without thick steel plates at the top and the bottom, so they rely essentially on friction from the isolator to the superstructure and foundations.^[5]

Unbounded FREI specimens reinforced by twisted stands of Kevlar were constructed and tested at the Pacific Earthquake Engineering Research Centre, Berkeley.^[4] In unfixed FREIs, the total thickness of the rubber (t_r) is almost equal to the height of the bearing (h), as the total thickness of the fiber sheets is negligible compared with the thickness of the elastomer. Experimental results show that the vertical stiffness of FREI, which makes the isolator stable against large vertical loads, is $\approx 20\%$ less than the equivalent for SREI.^[4] These results

Dr. M. R. Marsico, Dr. J. M. Londoño Monsalve, Dr. D.-W. Shin, Prof. M. F. Craciun
 College of Engineering, Mathematics and Physical Sciences
 University of Exeter
 Exeter EX4 4QF, UK
 E-mail: m.r.marsico@exeter.ac.uk

 The ORCID identification number(s) for the author(s) of this article can be found under <https://doi.org/10.1002/adem.201900852>.

© 2020 The Authors. Published by WILEY-VCH Verlag GmbH & Co. KGaA, Weinheim. This is an open access article under the terms of the Creative Commons Attribution License, which permits use, distribution and reproduction in any medium, provided the original work is properly cited.

DOI: 10.1002/adem.201900852

do not compromise the stability of FREIs as they are stable up to a peak shear strain of 150%, but they raise concerns whether it is possible to produce FREIs with the same (or higher) load capability and flexibility as SREIs to undergo large horizontal displacements during a seismic event. It was also observed experimentally that fiber reinforcement adds significant frictional damping due to individual strands in the fiber bundle slipping against each other when a FREI is displaced in shear. This means that in an isolation system even lower modulus elastomers can be used, which reduces costs further.

Experimental studies have investigated crucial parameters of FREIs such as vertical stress, horizontal deflection, bearing height, number of layers of elastomer and reinforcement, reinforcement material, and damping coefficient. Strauss found that the stiffness of FREIs depends on the preloading situation; the fibers have the ability to align according to the loading direction; therefore, the material behavior is characterized as degradation dependent. This may be an uncertain parameter when the preloading situation of the fibers is unknown.^[2]

Numerous studies suggest the use of FREI in lieu of heavy SREI, albeit aspects such as design, alignment, and behavior of the fibers would require further investigation. In particular, the dependence of FREI to preloading history, fiber alignment, and pretension remain unclear, bringing uncertainty into the design, manufacturing, and performance of those devices.^[10]

An attractive alternative to use fibers to reinforce rubber is graphene. Graphene, a one-atom-thick layer of carbon, is one of the thinnest materials which can be conceived. It is the strongest known material, which is also mechanically flexible. The superior mechanical properties of graphene have already made this material a top candidate for various emerging applications from flexible electronics to provide unprecedented outstanding reinforcement in composites.^[11–13] Many studies were conducted to determine the mechanical properties, electrical conductivity, gas permeability, and thermal stability of this material; however, there are only a few works that incorporate graphene into elastomers. For instance, Prud'Homme et al. added thermally reduced graphene into several elastomers, and their work demonstrates the prominent potential of graphene in improving the mechanical properties of elastomers.^[14] Wu et al. studied the influence of graphene on the vulcanization kinetics of natural rubber with sulfur curing system, and observed that graphene can be used to tune the vulcanization kinetics of rubbers.^[15]

The idea behind the research presented in this article is to reinforce pure rubber with a few-layer graphene and to create graphene-reinforced EI (GREI), which have to be stiffer vertically than horizontally to accommodate earthquake-induced vibrations to structures. This research also aims at exploiting the properties of graphene to enhance the damping of the graphene–rubber compound. Additional damping in the graphene–rubber compound will open the possibility of using pure rubber in lieu of high damping rubber reinforced with special particles; this will further lead to cost saving of those devices. The dynamic response of square and circular graphene–rubber specimens with applied vertical load is investigated. In Section 2, the composition of the specimens and the experimental setup are described. In Section 3, the theoretical background is presented. In Section 4, experimental results are analyzed and discussed.

2. Composition of Specimens and Experimental Setup

2.1. Description of the Specimens

Graphene deposition on rubber was achieved by a transfer method we have developed recently, isopropyl alcohol (IPA)-assisted direct transfer method (IDT).^[16] Specifically, a graphene film consisting of a random network of nanosheets was first deposited on a filter membrane (Milipore, hydrophilic polytetrafluoroethylene [PTFE] with 200 nm pores and 47 mm diameter) and then transferred onto rubber by IDT at 50 °C due to IPA evaporation (see our previous work for the details of transfer mechanism^[16]), as shown in **Figure 1a**. Few-layer graphene nanosheets, composing the graphene film on rubber, were prepared in water by shear exfoliation technique (**Figure 1b**).^[16,17] In this technique, a mechanical force produced by rotating the rotor inside the high shear mixer head allows for the liquid-phase exfoliation of graphite flakes (Sigma-Aldrich, 332461) into ultrathin few-layer graphene nanosheets (the scheme in **Figure 1b**). Sodium cholate, which is an amphiphilic surfactant, was used to settle the exfoliated few-layer graphene nanosheets in water (red dots covered graphene sheet in the scheme of **Figure 1b**). The water-exfoliated graphene solution was obtained after shear exfoliation at 4500 rpm for 60 min and a centrifugation process at 1500 rpm for 100 min to remove the unexfoliated graphite.^[16] Graphene films were initially obtained on a membrane by vacuum filtration of 15 mL of graphene solution (image panel in right-down side of **Figure 1b**) and then transferred onto rubber. To vary the thickness of the graphene films on rubber, multiple transfers of graphene films were used (i.e., three transfers for the thin films and six transfers for the thick films). The crystallinity of graphene nanosheets was characterized by Raman spectroscopy (using a custom-built setup^[18] based on an Olympus coupled to Princeton Instruments ACTON-SP2500 spectrometer [1800 g mm⁻¹, 500 nm Blaze] with a PIXIS-400 eXcelon charge-coupled devices) and X-ray diffraction (XRD; the Bruker D8 advanced XRD), as shown in **Figure 1c,d**. The Raman spectra in **Figure 1c** show the characteristic peaks of sp² bonded carbon atoms: the D-peak at ≈1340 cm⁻¹, the G-peak around 1600 cm⁻¹, the D'-peak around 1620 cm⁻¹, and the 2D-peak at ≈2700 cm⁻¹. The position of defects that could be induced in graphene by shear exfoliation can be estimated by the intensities ratio of D- and D'-band in the Raman spectra.^[16,17] We obtained $I(D)/I(D') \approx 4.7$, which means that graphene has most edge defects and few defects on the basal plane of graphene, but we note that the contribution of defects on the basal plane is not introduced by shear exfoliation process because graphene flakes already have basal plane defects ($I(D)/I(G) \approx 0.0555$). In addition, we observed a high crystalline quality of graphene film by XRD, obtaining 26.6° peak same as a main peak position of graphite, which is in agreement with previous Raman and X-ray photoelectron spectroscopy (XPS) data. **Figure 1e** shows the atomic force microscopy (AFM; the Bruker Innova AFM system in tapping mode) image of stacked few-layer graphene nanosheets prepared on SiO₂/Si substrate. The average number of layers and nanosheet lateral size of graphene is four layers and ≈110 nm, respectively, and has been reported elsewhere.^[16] We observed aggregated few-layer graphene nanosheets to form film with

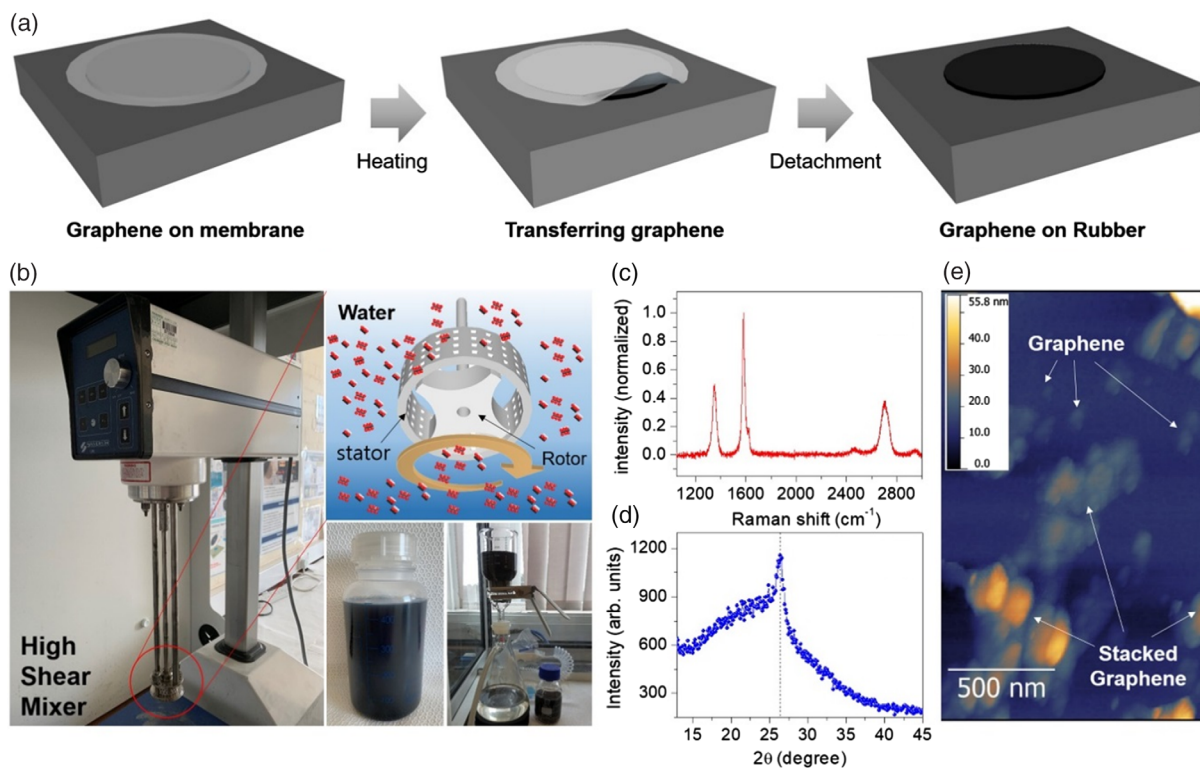


Figure 1. Preparation of water exfoliated graphene solution, transfer of graphene on the rubber, and its characterization. a) The scheme of transfer of graphene from the filter membrane to the rubber. b) The photo images of high shear mixer, graphene solution obtained, and vacuum filtration that allows to initially deposit graphene film on the filter membrane. The scheme of exfoliated graphene nanosheets with NaC in water due to a shear force caused by the holes of the stator and rotating the rotor. c) Raman and d) XRD spectra of graphene film. e) AFM images of graphene film.

the random networks. **Figure 2** shows two square rubber pads with thick and thin layers of graphene on top.

To study the influence of the shape factor, which is a dimensionless measure of the aspect ratio of the single layer of the elastomer and it is defined as the ratio between loaded area and force-free area, we have manufactured two sets of samples, with circular and square geometries. Set 1 samples are confined to two 72×72 mm square steel plates with 3 mm thickness, whereas Set 2 samples are confined to two circular steel plates with 3 mm thickness and 72 mm diameter.

Set 1 consists of three specimens. Specimen 1.1 is made of a square pure rubber pad of 47 mm side and 15 mm thickness; specimen 1.2 is made of a square rubber pad of 47 mm side and 15 mm thickness with a circular thick layer of graphene on the top with a diameter of 38 mm; and specimen 1.3 is made of a square rubber pad of 47 and 15 mm-thick side with a circular thin layer of graphene on the top with a diameter of 38 mm.

Set 2 consists of two specimens made of nine circular pads of rubber each with a diameter of 47 mm and thickness of 1.5 mm. Specimen 2.1 is made of nine pads of pure rubber bonded together using a cold vulcanizing agent. Specimen 2.2 is made of nine pads of rubber alternated to eight circular thin layers of graphene with a diameter of 38 mm. Thin layers of graphene were transferred upon the rubber pads using ≈ 45 mL of graphene solution in water solvent. Rubber pads with graphene on top were bound one another using a cold vulcanizing agent.

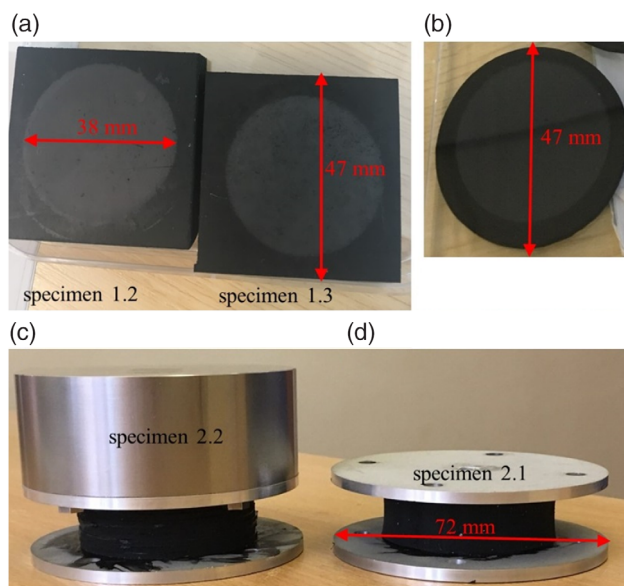


Figure 2. a) Specimens 1.2 and 1.3 made of a square rubber pad (15 mm thick), with thick (left) and thin (right) layers of graphene transferred on top. b) Circular sample: 1.5 mm thick rubber pad with a few-layer graphene on top. c) Specimen 2.2: nine circular rubber pads with diameter of 47 mm and thickness of 1.5 mm reinforced with eight layers of graphene and 1 kg vertical load. d) Specimen 2.1: nine circular rubber pads.

Figure 2 shows circular specimens 2.1 and 2.2 (Figure 2a,b), an enlargement of specimen 2.2 (Figure 2c) and a 1.5 mm rubber pad with graphene transferred on top (Figure 2d) that is repeated 9 times to make specimen 2.2.

The total height of the specimens (h) is assumed equal to the thickness of the rubber that is 15 mm for Set 1 and 13.5 mm for Set 2 samples. Indeed, the thickness of a few-layer graphene t_g transferred on top of the rubber pad is negligible (a ten-layer graphene film is ≈ 4.61 nm). The elastomer used in Sets 1 and 2 samples is natural rubber with hardness 70° Shore A Degree, measured experimentally using a RS Pro digital durometer with application range of 10–90 Shore A unit and ± 1 hardness unit accuracy. Sets 1 and 2 samples were cured for 15 days at room temperature of approximately 20° before being tested.

2.2. Experimental Setup

The experimental setup shown in Figure 3a can be seen as a single-degree-of-freedom (SDOF) mass-spring-damper system (Figure 3b). M is the load applied on a specimen, and K and ζ are the stiffness and the damping of the specimen; \ddot{x}_1 is the acceleration recorded at the bottom of the lower steel plate bonded to the specimen and \ddot{x}_2 is the acceleration recorded at the top of the added mass. Initial tests were conducted on three Set 1 square samples, and the second sequence of tests was conducted on two Set 2 circular samples described in Section 2. Experimental modal analysis was performed on the mass-spring-damper system and the dynamics of the system and the mechanical properties essential to characterize the specimens were extracted from the measured frequency response function (FRF).

The experimental setup whose components are shown in Figure 3b consists of a vertical SignalForce Shaker V20 applying dynamic loading to the bottom of the specimen. A load cell (PCB Piezotronics 208C02) is attached to the bottom steel plate of each specimen to measure the vertical forces effectively transmitted from the shaker; gravity loads are applied on the specimens

in the form of a solid stainless steel cylinder bolted to the upper steel plate (1 and 2 kg at a time). Two accelerometers, a PCB Piezotronics M353B18 at the top and a high sensitivity single-axis accelerometer KISTLER 8640A50 at the bottom, were used to record accelerations (in grams) at the top of the added mass (stainless steel cylinder) and at the bottom of the lower steel plate, respectively. LabVIEW software was used to acquire and process experimental data.

Initial tests conducted at the Dynamics Laboratory of the University of Exeter (UK) aimed at determining the dynamic properties of the specimens. To measure their resonance frequency, specimens were loaded using sine-sweep excitation within a frequency range of 0–5000 Hz, with an input amplitude of 0.2 root-mean-square voltage (VRMS). To reduce the presence of measurement noise on the FRF estimates, RMS spectral averaging was performed on ten spectral records (computing the square root of the average of the sample values squared) and each spectral record was weighted using linear weighting, which combines spectral records with equal weighting. Vibration tests were also performed on one of the 3 mm steel plates alone to define its natural frequency and ultimately to assess any dynamic interaction with the dynamic behavior of the rubber–graphene compound. Figure 3c shows the experimental setup for tests conducted on a square steel plate. An accelerometer is positioned at the top of the plate and a load cell is at the bottom to record the applied force.

3. Damping, Vertical Stiffness, and Compression Modulus in the Graphene–Rubber Composite

The natural frequency and damping of the specimens were initially estimated from the FRF using the peak-picking and half-power bandwidth methods. Peak picking is a method operating in the frequency domain where each peak corresponds to one natural mode and it is applicable when the modes of the system are well separated in the frequency domain. Half-power

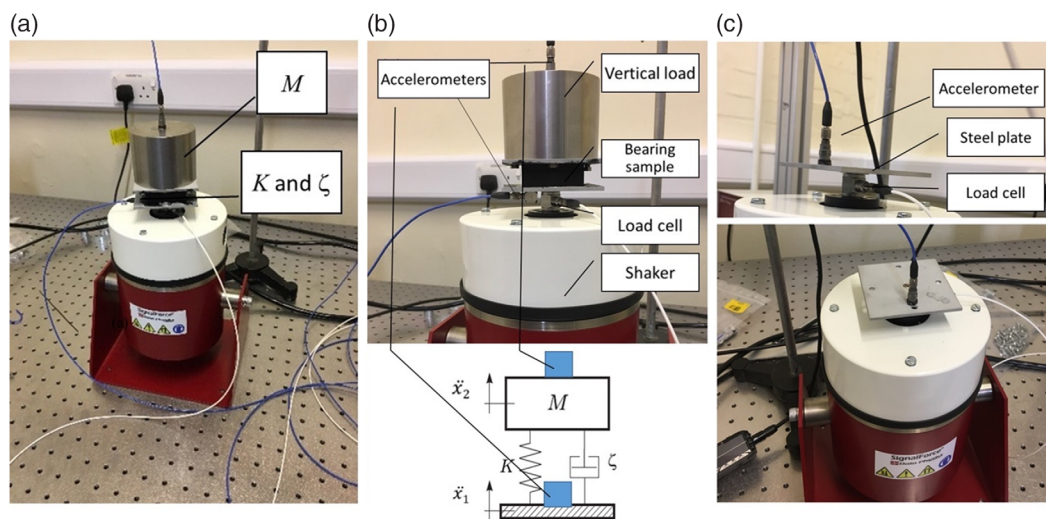


Figure 3. a) Experimental setup; b) corresponding SDOF mass-spring-damper system. Components of the experimental setup. c) Experimental tests conducted on a square steel plate of 3 mm thickness.

bandwidth is based on the assumption that the damping of a system ζ is proportional to the width of the resonant peak about the peak's center frequency.^[19] The natural frequency of Sets 1 and 2 samples is estimated experimentally via FRF, and the damping ratio ζ of the mass-spring-damper system is calculated using the equation

$$2\zeta = \eta \quad (1)$$

where

$$\eta = (f_b^2 - f_a^2)/(2f_n^2) \quad (2)$$

and where f_n is the frequency of resonant peak in hertz; f_b is the higher frequency at amplitude $H/\sqrt{2}$; f_a is the lower frequency at amplitude $H/\sqrt{2}$; and H is the amplitude of the response at f_n .

The damping estimated using Equation (1) was compared with the damping estimated using the least-squares fitting rational function (LSRF) approach.^[20] LSRF is an estimation-based method fitting data by rational functions that minimize the maximum error between the fitting function and the data. It provides higher-accuracy results for single-input–single-output (SISO) frequency-domain systems with real-valued state-space parameters, therefore applicable to the observed SDOF mass-spring-damper system. The linearity of the experimental system and the dominance of the first mode were verified on a Nyquist diagram—plotting real versus imaginary data of FRFs.

To define the vertical stiffness K_v of Sets 1 and 2 samples, a rearranged equation of an SDOF system is used

$$K_v = 4\pi^2 f_n^2 M \quad (3)$$

where f_n is the experimental vertical natural frequency and M is the applied mass. Knowing the vertical stiffness K_v , the instantaneous compression modulus E_c of the specimen is calculated from the theory developed by Kelly and Takhirov for FREIs^[4]

$$E_c = \frac{K_v \cdot t_r}{A} \quad (4)$$

where A is the cross-sectional area of the bearing and t_r is the total thickness of rubber in the device. For the Set 2 circular specimens, the cross-sectional area is $A = \pi d^2/4$, where d is the diameter of the circular rubber pad (47 mm); for the Set 1 square specimens, the cross-sectional area is $A = a^2$, where a is the side of the square rubber pad (47 mm).

Values of vertical stiffness and instantaneous compression modulus of the graphene–rubber composite are shown in Table 1 and 2, and are discussed hereinafter.

4. Analysis of Experimental Results

4.1. Results on Set 1 Specimens (Square)

FRFs of Set 1 samples were used to evaluate the specimens' mechanical behavior and to extract dynamic properties such as the natural frequency and damping. FRFs show that the vertical natural frequency of the two specimens 1.2 and 1.3 made of a rubber pad and a few-layer graphene on top (either thin or thick)

Table 1. Mechanical properties of three specimens made of a rubber pad (specimen 1.1), a rubber pad with a thick layer of graphene on top (specimen 1.2), and a rubber pad with a thin layer of graphene on top (specimen 1.3).

	Rubber pad (specimen 1.1)	Rubber pad + graphene thick layer (specimen 1.2)	Rubber pad + graphene thin layer (specimen 1.3)
Natural frequency f_n [Hz]	315	338	340
Cross-over frequency [Hz]	452	493	501
Damping factor ζ (peak picking)	0.1236	0.1245	0.1455
Vertical stiffness [N m ⁻¹] (SDOF)	3 942 157	4 510 172	4 590 590
Increase vertical stiffness [%]	–	14.41	16.45
Instantaneous compression modulus E_c [N m ⁻²]	3.41E+07	3.90E+07	3.97E+07
LSRF method			
Natural Frequency f_n [Hz]	318	344	348
Damping factor ζ	0.1212	0.1233	0.1292

is higher than the natural frequency of the specimen made of pure rubber (1.1). This result proves that specimens 1.2 and 1.3 are stiffer vertically than specimen 1.1, and that the increase in vertical stiffness is likely due to the added layers of graphene. Layers of graphene act as reinforcements: by restricting the freedom of the rubber to bulge, and by inducing tensile stresses during their action in limiting the bulging, and therefore, enhancing the vertical stiffness of the elastomer. The vertical natural frequency of the three specimens is shown in Figure 4, also showing that for exciting frequencies less than 250 Hz (i.e., a frequency ratio less than 0.7) the dynamic response of the specimens is disturbed by the dynamic response of the confining steel plates. Despite this, the disturbance does not compromise the experimental measurements because it occurs at an outer frequency away from the natural frequencies of the three specimens. The resonance frequency estimated experimentally from FRF was compared with the resonance frequency estimated using the LSRF approach described in Section 3 and it was found to be within one percentile difference for specimen 1.1 and two percentile difference for specimens 1.2 and 1.3. LSRF stabilization diagrams are shown in Figure 5 and confirm that specimens 1.2 and 1.3 have natural frequencies higher than specimen 1.1. Those results show that the LSRF approach gives reliable results for the SDOF system investigated here. Results are encouraging: seismic elastomeric devices would require very high vertical stiffness compared with the horizontal one and graphene appears to be a viable alternative to replace steel shim in SREI (or fibers in FREI) and to provide the required increase in the vertical stiffness. In addition, the use of graphene in seismic devices will reduce the weight of the devices further, therefore costs.

This article is devoted to test graphene rubber compounds to be used for prototypes of EIs able to isolate structures from vibrations. Isolation of structures from external excitation occurs for the ratio of the output signal (i.e., accelerations recorded at the top of the added mass M) to the input signal (i.e., accelerations

Table 2. Mechanical properties of Set 2 samples.

	Round rubber layers with 1 kg (specimen 2.1)	Round graphene–rubber layers with 1 kg (specimen 2.2)	Round rubber layers with 2 kg (specimen 2.1)	Round graphene–rubber layers with 2 kg (specimen 2.2)
Resonance frequency [Hz]	506	271	345	205
Damping factor ζ (peak picking)	0.273	0.183	0.293	0.2013
Energy loss in the hysteresis loop [%]	1.00	4.89	1.00	4.27
Experimental Young's modulus E_{ex} [$N\ m^{-2}$]	1.00E+09	2.60E+08	8.50E+08	2.71E+08
Instantaneous compression modulus E_c [$N\ m^{-2}$]	7.87E+07	2.26E+07	7.31E+07	2.58E+07
Vertical stiffness [$N\ m^{-1}$] (SDOF)	1.01E+07	2.90E+06	9.40E+06	3.32E+06

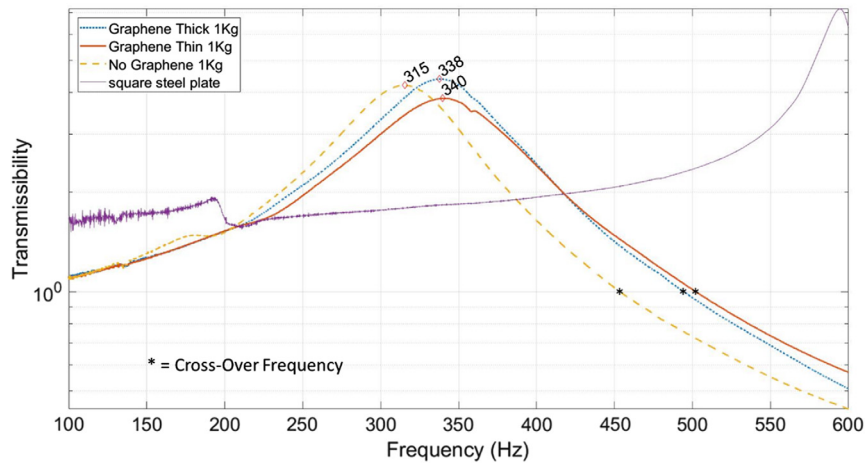


Figure 4. Set 1 samples: transmissibility and cross-over frequency at $T = 1$.

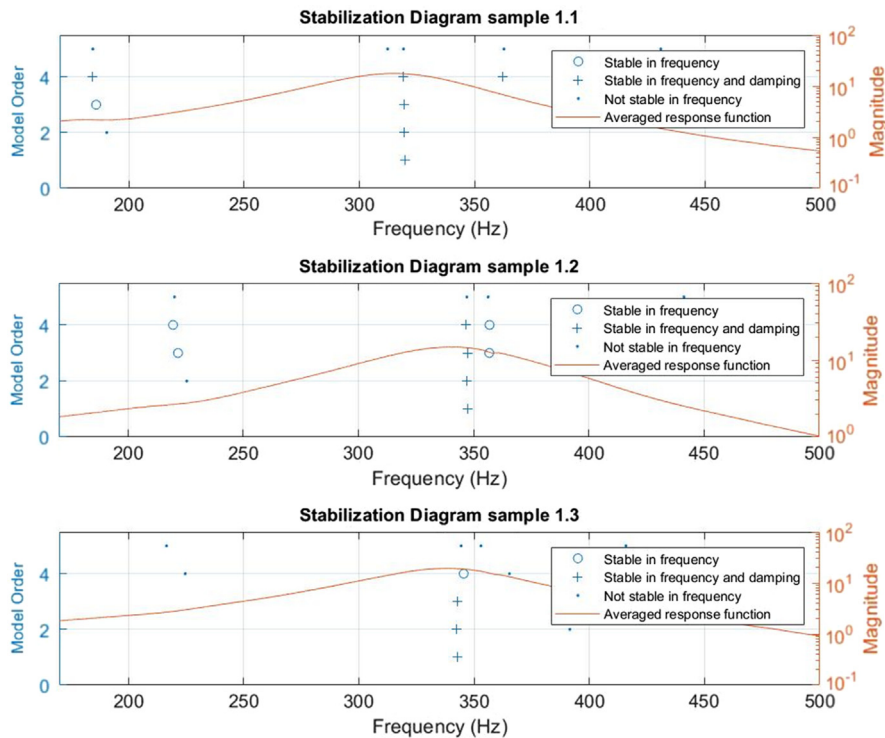


Figure 5. Stabilization diagram of Set 1 samples.

recorded on the lower steel plate) less than 1; it is known as transmissibility T . The cross-over frequency at $T = 1$ for the three Set 1 samples is shown in Figure 4, showing that for a given value of transmissibility less than 1, the specimen 1.3 (with thin layer of graphene) isolates a structure from higher frequencies than specimens 1.1 and 1.2. From Figure 4, it is also evident that for high-frequency ratios (i.e., exciting frequency to frequency of the mass-spring-damper system), the transmissibility is not strongly dependent on the loss factor (i.e., damping). This confirms that the hysteretic model suggested by Kelly is the most appropriate theoretical model to describe the behavior of rubber material reinforced with graphene as it predicts a larger degree of dynamic isolation at high-frequency ratio than do other models (e.g., viscous model).^[1] Therefore, the hysteretic model can be extended to graphene-reinforced compounds, although further amendments will be essential, as discussed in Section 4.2.^[1,4] Indeed, the unprecedented concept of replacing steel shims with few-layer graphene nanosheets to make GREI demands the development of a bespoke theoretical model on which the authors are currently working.

Damping ratio of Set 1 samples, estimated using the method described in Section 3, is shown in Table 1. Results show that by adding a few layer of graphene on a rubber pad, the damping factor ζ increases from 0.12 (in specimen 1.1) to 0.15 (in specimen 1.3). This result is compared with high-damping SREI, also known as high-damping steel reinforced rubber bearings (HDRB), for which the characteristic damping factor is between 0.1 (10%) and 0.2 (20%). For instance, results from tests presented by Nersessyan et al.^[21] show that HDRB with filled natural rubber have $\zeta \approx 0.14$ (14%), which is a typical value for seismic EIs. This value is very close to the damping of specimen 1.3, proving that in a natural rubber pad reinforced with a thin layer of graphene it is relatively easy to achieve the damping ratio of high damping rubber. Such an increase in damping ratio is likely due to the presence of graphene and it is beneficial to vibration isolation systems made with rubber, as it would enable using low damping natural rubber in lieu of expensive high damping rubber (requiring an additional manufacturing process to be filled with reinforcing particles). Results also show that increasing the quantity of graphene in the graphene–rubber compound

does not necessarily correspond to an increase in damping. For instance, specimen 1.2 has more graphene (thick layer) but a lower damping ratio than specimen 1.3. Therefore, it is crucial to study the relationship between the quantity of graphene added on rubber and the properties of the graphene–rubber compound.

Experimental data from FRF were plotted on the Nyquist plane and they appear to distribute properly on a circle generated using a circle fit method. Such a distribution corroborates the hypothesis that the analyzed system is behaving linearly and has one significant natural frequency. **Figure 6** shows Nyquist planes for the three Set 1 samples with 1 kg vertical load applied.

The instantaneous compression modulus E_c of the graphene–rubber compound is calculated from Equation (4). E_c increases with the vertical stiffness; therefore, it is greater in specimens 1.2 and 1.3 than in specimen 1.1. Experimental value of instantaneous compression modulus of Set 1 samples are shown in Table 1.

It is worth noting that an increase in concentration of graphene (from thin to thick layer) does not enhance further natural frequency and damping factor. Recent studies found similar results with respect to the evolution of functionalities of graphene composites by varying concentration of graphene.^[11,12] In nanoengineered concrete reinforced with graphene, it was observed an increase in strength and of a range of mechanical properties (e.g., compressive strength and flexural strength); yet a further increase in graphene concentration in the reinforced concrete reduces some of them (e.g., plastic strain). This demanded a systematic study on the graphene reinforced concrete to investigate the evolution of its functionalities. Research studies also demonstrated that strength in graphene–elastomer nanocomposite is sensitive to preparation techniques, many of which can be used only for the incorporation of small amounts of graphene because the use of higher amounts can easily lead to an increase in the cross-link density of the elastomer, which will diminish the effect of the functionalization. It follows that the preparation of Set 2 specimens and their peculiar geometry (alternated layers of rubber and graphene) may have produced microstructural changes weakening the specimens and affecting their mechanical properties.

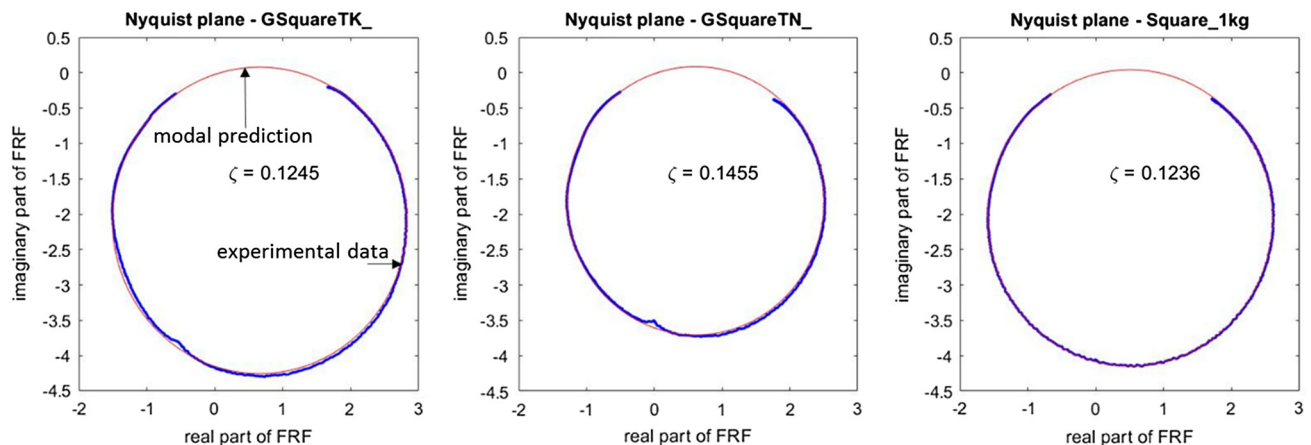


Figure 6. Nyquist plane for the three Set 1 samples with 1 kg vertical load.

4.2. Results on Set 2 Specimens (Circular)

In this section, experimental results from dynamic tests conducted on two circular specimens (specimens 2.1 and 2.2) with 1 and 2 kg vertical load applied one at a time are presented and discussed. The vertical natural frequency of the two specimens was found using the experimentally measured FRF. The natural frequency in the specimen made of nine rubber pads (specimen 2.1) was found to be higher than the frequency of the specimen made of rubber pads alternated with eight layers of graphene (specimen 2.2). This may indicate that eight layers of graphene are added at the expenses of the vertical stiffness of the layered specimen. Vertical natural frequency of Set 2 samples is shown in **Figure 7**, also showing the transmissibility. As the natural frequency is lower in specimen 2.2 than in specimen 2.1, the vertical stiffness calculated experimentally from the mass-spring-damper SDOF system is also lower in the graphene-reinforced rubber specimen compared with that in the specimen made of rubber pads only. In addition to that, experimental results indicate a lower damping factor (calculated using the pick peaking method discussed in Section 3) of the specimen reinforced with graphene compared with the damping factor of the specimen made of rubber pads only. Such a decrease in

vertical frequency, vertical stiffness, and damping factor in the specimen reinforced with graphene is likely due to an excessive quantity of graphene present in the specimen 2.2, provoking loss of adhesion between layers of graphene-reinforced rubber and unexpected inner behavior between the graphene particles.

Results on tests conducted on Set 2 samples reaffirm those on Set 1 samples and in particular on specimens 1.2 and 1.3. Indeed, the mechanical properties of specimen 1.2 (with a thick layer of graphene), e.g., natural frequency, damping, vertical stiffness, and instantaneous compression modulus, are inferior to the properties of the specimen 1.3 (with thin layer of graphene) indicating that high concentration of graphene weakens the specimen. A comprehensive overview of the experimental results for Set 2 samples is shown in Table 2.

To design a base isolated system, it is essential to know the instantaneous compression modulus E_c of the EIs. Here, E_c is calculated using the theory developed by Kelly and Takhirov;^[4] then, it is compared with the compression modulus E_{ex} extracted from the experimental hysteresis loop, defined as the ratio between the tensile stress (σ) and the vertical deformation (ϵ), such as

$$E_{ex} = \frac{\sigma}{\epsilon} \quad (5)$$

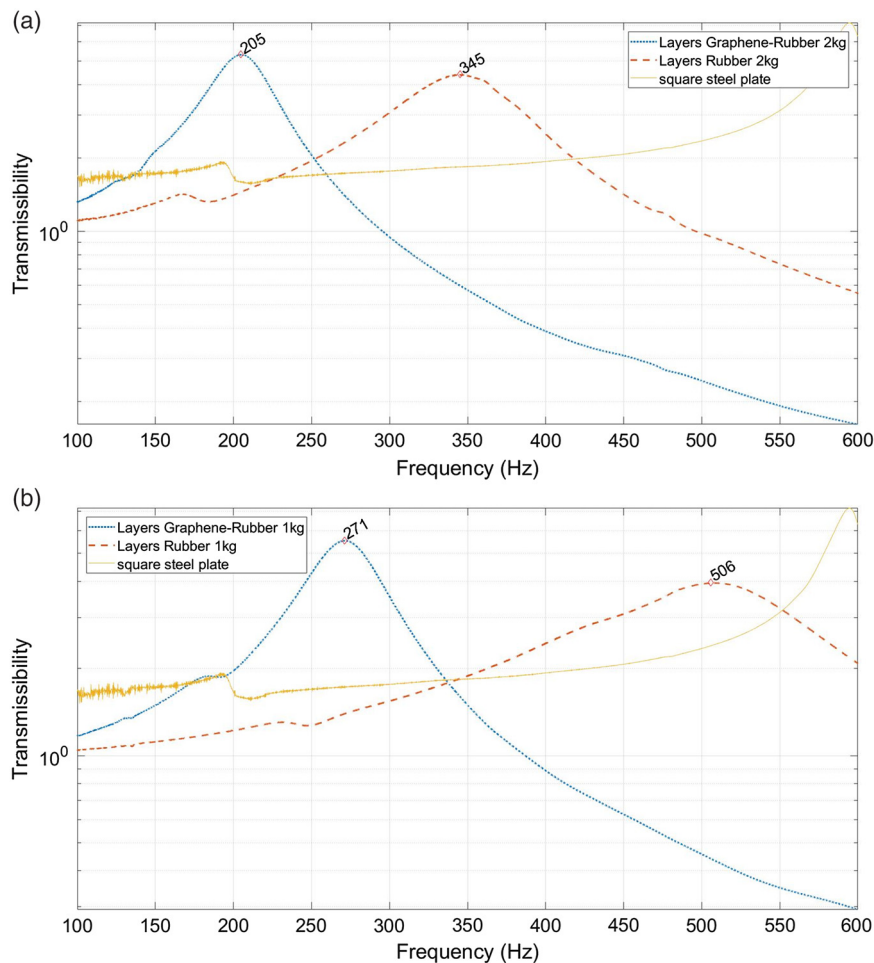


Figure 7. Transmissibility of Set 2 samples: a) specimens with vertical load of 1 kg; b) specimens with vertical load of 2 kg.

The tensile stress σ is calculated as

$$\sigma = F/A \quad (6)$$

where F is the force applied on the sample by the vertical shaker and recorded at the bottom of the lower steel plate and A is the cross-sectional area of the sample. The vertical deformation ϵ is calculated as

$$\epsilon = \Delta l/l \quad (7)$$

where Δl is the relative displacement such as the difference between the displacement recorded at the bottom of the lower steel plate and the displacement recorded at the top of the specimen; l is high for Set 2 samples ($h = 13.5$ mm). Accelerations recorded by two accelerometers were integrated to extract the vertical displacements of the specimens, and a filter was applied to remove baseline errors accumulated in the numerical integration.

The experimental Young's modulus E_{ex} is about 10 times greater than the instantaneous compression modulus E_c calculated using the theory developed for FREI.^[4] This result shows that the models discussed by Kelly and Takhirov^[4] are not a comprehensive representation of the mechanical behavior of GREI; additional experimental tests are essential to develop a theory to better describe the dynamic behavior of GREI. Despite inconsistency between E_c and E_{ex} , specimen 2.2 with either 1 or 2 kg applied load has lower E_c than the specimen made of rubber pads only (specimen 2.1). This confirms that an excessive quantity of graphene in the specimen (i.e., eight layers of graphene in specimen 2.2) is likely to worsen its mechanical properties and that although there is evidence that graphene enhances the properties of rubber, it is essential encountering the optimal quantity.^[12] In addition, specimens were handmade and it was observed that the epoxy that was used to bind the layers of rubber was too dense, and it creates microcavities that prevent the rubber pads to adhere uniformly to one another. Both Set 2 samples were excited at their natural frequency and σ - ϵ plots are shown in **Figure 8**.

To compare the hysteresis loops and evaluate the energy losses in load-unload cycles, specimens 2.1 and 2.2 were excited at their natural frequency and equal amplitudes. The relative vertical displacement is experimentally estimated using the difference between the displacement at the top minus the displacement at the bottom of the specimen. **Figure 9** plots the relative vertical displacement versus the forces effectively transmitted from the shaker.

Overall, specimen 2.1 loses much more energy (as a consequence of its higher damping) than specimen 2.2. For instance, the energy loss in load-unload cycles of specimen 2.2 (**Figure 9d**) is about 8.5% less than the energy loss in load-unload cycles of specimen 2.1 (**Figure 9c**). This again confirms that despite graphene layers that enhance the properties of the rubber pads (specimens 1.2 and 1.3), an excessive quantity of graphene, which in this case is due to the presence of eight layers of graphene, may be counterproductive for an isolation system. Therefore, it is essential to determine the optimal quantity of graphene to be transferred on rubber pads to design an efficient isolation system.

5. Conclusions

Typically, seismic EIs are made with high damping rubber to reduce further horizontal accelerations induced in structures during an earthquake, and are reinforced with steel plates that provide large vertical stiffness. Experimental results conducted on the three Set 1 samples with 1 kg vertical load applied showed that while adding a few-layer graphene on the top of a 15 mm-thick rubber pad, the vertical stiffness of the specimen increases. In particular, the vertical stiffness increases by 16.5% when a thin layer of graphene is added on the top of the rubber pad and by 14.4% when a thick layer of graphene is added.

Experimental results also show an increase in 17.7% in the damping of the composite rubber thin layer of graphene (specimen 1.3) and of 0.7% in the composite rubber thick layer of graphene (specimen 1.2). Thick and thin layers of graphene are

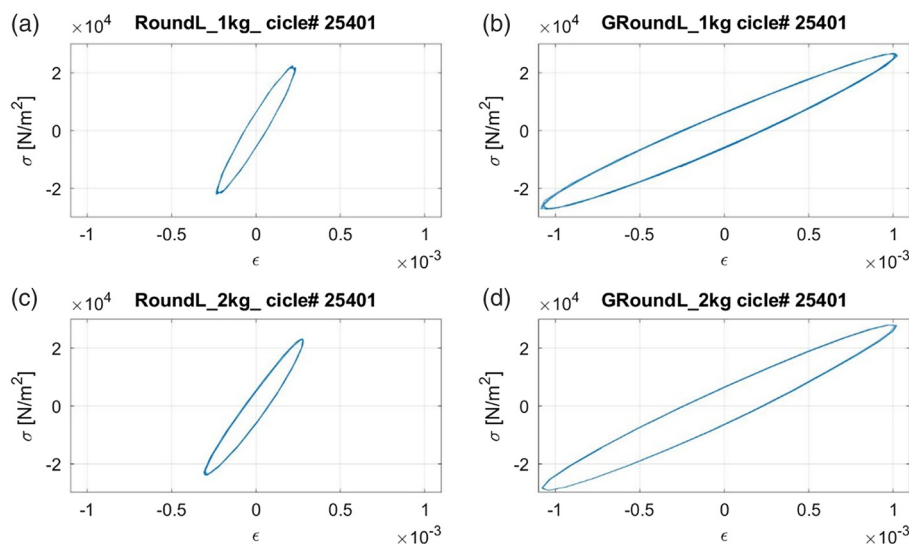


Figure 8. Young's modulus E_{ex} for Set 2 samples. a) Specimen 2.1 under 1 kg; b) specimen 2.2 under 1 kg; c) specimen 2.1 under 2 kg; d) specimen 2.2 under 2 kg.



Figure 9. Relative vertical displacement versus effectively applied force. a,d) Specimen 2.1 and specimen 2.2 when excited at their respective natural frequencies; b) specimen 2.2 when excited at its natural frequency with amplitude as produced by specimen 2.1 in (a); c) specimen 2.1 when excited at its natural frequency with amplitude as produced by specimen 2.2 in (d).

produced by varying the quantity of graphene solution in water solvent. Results also show that a few-layer graphene transferred on top of the specimen enhances the damping; therefore, natural rubber can be used in lieu of high damping rubber, saving the cost of reinforcing rubber with particulate fillers. Adding a few-layer graphene is proved to be a viable and low-cost alternative to reinforce EIs and to replace heavy steel reinforcing shims.

The rubber pad with a thick layer of graphene on top is shown to be less performant than the rubber pad with a thin-layer graphene. This is likely due to an excessive quantity of graphene concentration used to make the graphene layer thick, causing unexpected behavior of the graphene particles and loss of chemical bounds.

Unwanted behavior of the rubber pad due to high concentration of graphene is evident from the experimental results on Set 2 samples. The specimen made with nine rubber pads alternated with eight layers of graphene exhibits lower vertical stiffness and damping factor than the specimen made of nine rubber pads only. Eight layers of graphene worsen the performance of the rubber, although it is likely that less layers would enhance its mechanical properties, as it is seen in the response of specimen 1.3 with a thin layer of graphene on top. An increment in vertical stiffness was expected in specimen 2.2 (GREI) with respect to specimen 2.1, similar to the increment that was observed in specimen 1.3 with respect to specimen 1.1. This would be achieved by transferring the optimal quantity of graphene on the rubber pads. Using the theory developed by Kelly^[1] and assuming a compression modulus $G = 0.4$ MPa which is a typical value in SREI, it is possible to design a SREI with the same vertical stiffness as GREI. It would have 15 layers of steel shims interposed between 16 layers of 1.5 mm rubber.^[1] Therefore, a SREI would be heavier and taller than GREI, proving that a GREI with optimal concentration of graphene would match the mechanical properties of a typical SREI, as well as being lighter and therefore easier to transport and install. The quest for future research is to determine the

optimal quantity of graphene to be transferred homogeneously on the rubber pad that would enhance its mechanical properties.

It is worth mentioning that Sets 1 and 2 samples were handmade and the epoxide used to bind layers of rubber (and layers of reinforced rubber) was dense and could have not adhered homogeneously on the surface, causing an amount of scatter and microstructural changes weakening the specimens and their mechanical properties.

These results lay the foundation for expanding this research into a new generation of building-protection devices known as seismic metamaterials.^[22,23] For instance, GREI could be integrated with composite foundations that use the physics of seismic metamaterials to create onsite filters that reduced the energy transferred from a seismic wave to the building. Also, they could be used in the realization of periodic foundations which use periodic materials (e.g., phononic crystal) to change the pattern of the earthquake's energy and reduce the response of the upper structure from excitations within the frequency band of interest.

Acknowledgements

The authors acknowledge financial support from EPSRC (grant nos. EP/J000396/1, EP/K017160, EP/K010050/1, EP/G036101/1, EP/M002438/1, and EP/M001024/1) and the Royal Academy of Engineering.

Conflict of Interest

The authors declare no conflict of interest.

Author Contributions

M.R.M. conceived the project, designed the experiments, prepared and tested the samples, and analyzed the results. J.M.L.M. designed and performed the experiments, prepared and tested the samples, and analyzed

the results. D.W.S. transferred a few-layer graphene on rubber pads. M.F.C. provided the graphene samples and contributed to interpreting the results. M.R.M. and J.M.L.M. wrote the article with input from all authors.

Keywords

frequency response functions, graphene-reinforced elastomeric isolators, seismic isolation, vertical excitation

Received: July 17, 2019

Revised: February 26, 2020

Published online: March 26, 2020

-
- [1] J. M. Kelly, *Earthquake-Resistant Design with Rubber*, Springer, London **1997**.
- [2] A. Strauss, *Eng. Struct.* **2014**, *75*, 402.
- [3] L. Scott, *Engineering News Record*, <https://www.enr.com/articles/42366-the-10-largest-base-isolated-buildings-in-the-world> (accessed: October 2018).
- [4] J. M. Kelly, S. M. Takhirov, *PEER 11*, University of California, Berkeley, CA **2002**.
- [5] P. M. Osgoee, M. J. Tait, D. Konstantinidis, *Eng. Struct.* **2017**, *137*, 245.
- [6] J. M. Kelly, D. Konstantinidis, *Mechanics of Rubber Bearings for Seismic and Vibration Isolation*, John Wiley & Sons, Chichester, UK **2011**.
- [7] P. M. Osgoee, N. C. Van Engelen, D. Konstantinidis, M. J. Tait, *Eng. Struct.* **2015**, *85*, 293.
- [8] M. R. Marsico, J. M. Kelly, *Eng. Struct.* **2013**, *56*, 656.
- [9] P. Angeli, G. Russo, A. Paschini, *Int. J. Solids Struct.* **2013**, *50*, 3519.
- [10] A. E. Javid, J. Kelly, J. L. Sackman, *US Patent US5904010A*, **1999**.
- [11] D. Dimov, I. Amit, O. Gorrie, M. D. Barnes, N. J. Townsend, A. I. S. Neves, F. Withers, S. Russo, M. F. Craciun, *Adv. Funct. Mater.* **2018**, *28*, 1705183.
- [12] D. G. Papageorgiou, I. A. Kinloch, R. J. Young, *Carbon* **2015**, *95*, 460.
- [13] J. D. Wang, Y. F. Zhu, X. W. Zhou, G. Sui, J. Liang, *Appl. Polym. Sci.* **2006**, *100*, 4697.
- [14] R. K. Prud'Homme, B. Ozbas, I. Aksay, R. Register, D. Adamson, *US Patent US7745528B2*, **2010**.
- [15] J. Wu, W. Xing, G. Huang, H. Li, M. Tang, S. Wu, Y. Liu, *Polymer* **2013**, *54*, 3314.
- [16] D. W. Shin, M. D. Barnes, K. Walsh, D. Dimov, P. Tian, A. I. S. Neves, C. D. Wright, S. M. Yu, J. B. Yoo, S. Russo, M. F. Craciun, *Adv. Mater.* **2018**, *30*, 1802953.
- [17] K. R. Paton, E. Varrla, C. Backes, R. J. Smith, U. Khan, A. O'Neill, C. Boland, M. Lotya, O. M. Istrate, P. King, T. Higgins, S. Barwich, P. May, P. Puczkarski, I. Ahmed, M. Moebius, H. Pettersson, E. Long, J. Coelho, S. E. O'Brien, E. K. McGuire, B. Mendoza Sanchez, G. S. Duesberg, N. McEvoy, T. J. Pennycook, C. Downing, A. Crossley, V. Nicolosi, J. N. Coleman, *Nat. Mater.* **2014**, *13*, 624.
- [18] A. De Sanctis, J. D. Mehew, S. Alkhalifa, C. P. Tate, A. White, A. R. Woodgate, M. F. Craciun, S. Russo, *Rev. Sci. Instrum.* **2017**, *88*, 055102.
- [19] D. J. Ewins, *J. Vib. Acoust.* **1984**, *108*, 109.
- [20] A. A. Ozdemir, S. Gumosoy, *IFAC-PapersOnLine* **2017**, *50*, 6232.
- [21] T. Nersessyan, G. Hovhannissyan, A. Tonoyan, K. Avanesova, *J. Struct. Control* **2001**, *8*, 219.
- [22] Y. Yan, A. Laskar, Z. Cheng, F. Menq, Y. Tang, Y. L. Mo, Z. Shi, *J. Appl. Phys.* **2014**, *116*, 044908.
- [23] O. Casablanca, G. Ventura, F. Garesci, B. Azzerboni, B. Chiaia, M. Chiappini, G. Finocchio, *J. Appl. Phys.* **2018**, *123*, 174903.